Supporting Information for "Internal tides responsible for lithogenic inputs along the Iberian continental slope"

Simon Barbot[1], Marion Lagarde[1], Florent Lyard[1], Patrick Marsaleix[1],

Pascale Lherminier[2], Catherine Jeandel[1]

[1]LEGOS, Université de Toulouse, CNES, CNRS, IRD, UPS, Toulouse, France

[2]LOPS, Ifremer, Univ. Brest, CNRS, IRD, IUEM, Plouzané, France

Contents of this file

Introduction

Text S1 details the methodology for the calculation of the slope criticality. Text S2 details the feature used by the hydrodynamic numerical model SYMPHONIE and the specific choices that have been made for the BOBIBE configuration of this study. Figures S2 and S3 show validation of the barotropic and baroclinic tides for all the tidal harmonics used in the BOBIBE simulation. Figure S4 shows the validation of the IBIRYS12 reanalysis compared to GEOVIDE transect over co-located stations. Figure S5 details the impact of the average period used for the circulation to investigate the sediment transport. Table S1 lists the numerical and physical constants used for the BOBIBE configuration.

Text S1. Calculation of the slope criticality

The calculation of the critical slope is based on the ratio between the topography slope γ and the IT wave beam slope l. If $\gamma/c > 1$, the slope is considered as steep. If $\gamma/c > 1$, the slope is considered as flat. If $\gamma/c = 1$, the slope is considered as critical. The expression of c can be found from the dispersion relationship of the internal gravity wave in a rotating fluid (Kundu et al., 2004):

$$\omega^2 - N^2 \frac{k_H^2}{k_H^2 + k_V^2} + f^2 \frac{k_V^2}{k_H^2 + k_V^2} = 0 \tag{1}$$

with ω the wave frequency, N the Brunt-Vissl frequency, f the Coriolis parameter, k_H the horizontal wavenumber and k_V the vertical wavenumber. N is defined by the potential density profile:

$$N^2 = -\frac{g}{\rho_0} \frac{d\rho_0}{dz} \tag{2}$$

with g the gravitational acceleration, ρ_0 the unperturbed potential density. So for a given density profile, the IT wave beam slope can be calculated as the ratio between horizontal and vertical wavenumber:

$$c^2 = \frac{k_H^2}{k_V^2} = \frac{\omega^2 - f^2}{N^2 - \omega^2} \tag{3}$$

The calculation is made for M2, the dominant semi-diurnal tidal waves in this region. The diurnal tidal waves have no relevant criticality slope in this area because located outside the critical latitude ($f \geq \omega$).

Text S2. Numerical details of SYMPHONIE for the BOBIBE configuration

The numerical model SYMPHONIE[1] (Marsaleix et al., 2008, 2019) is based on the Navier-Stokes primitive equations solved on an Arakawa curvilinear C-grid (Arakawa & Lamb, 1981) under the hydrostatic and Boussinesq approximations. The model makes use of an energy conserving finite difference method described by Marsaleix et al. (2008), a forward-backward time stepping scheme, a Jacobian pressure gradient scheme (Marsaleix et al., 2009), the equation of state of Jackett, McDougall, Feistel, Wright, and Griffies (2006), and the K-epsilon turbulence scheme with the implementation described in Costa, Doglioli, Marsaleix, and Petrenko (2017). Horizontal advection and diffusion of tracers are computed using the QUICKEST scheme (Leonard, 1979) and vertical advection using a centered scheme. Horizontal advection and diffusion of momentum are each computed with a fourth order centered biharmonic scheme as in Damien, Bosse, Testor, Marsaleix, and Estournel (2017). The biharmonic viscosity of momentum is calculated according to a Smagorinsky-like formulation derived from Griffies and Hallberg (2000). The lateral open boundary conditions, based on radiation conditions combined with nudging conditions, are described in Marsaleix, Auclair, and Estournel (2006) and Toublanc, Ayoub, Lyard, Marsaleix, and Allain (2018).

The VQS (vanishing quasi-sigma) vertical coordinate described in Estournel, Marsaleix, and Ulses (2021) is used to avoid an excess of vertical levels in very shallow areas while maintaining an accurate description of the bathymetry and reducing the truncation errors associated with the sigma coordinate (Siddorn & Furner, 2013). The implementation of the tide, described in Pairaud, Lyard, Auclair, Letellier, and Marsaleix (2008); Pairaud, Auclair, Marsaleix, Lyard, and Pichon (2010), consists on the one hand of the amplitude

and phase of the tide introduced at the open lateral boundaries and on the other hand of the astronomical plus loading and self-attraction potentials.

In addition to this usual configuration of the model, specific nudging conditions have been developed for this particular study. To prevent the erosion of the stratification by the tides, a nudging term have been add in every point of the grid to maintain the initial value of temperature and salinity:

$$\frac{\partial X'}{\partial t} = ... + \lambda^R \bar{X}' \tag{4}$$

where X is the anomaly of either the temperature or the salinity, λ^R is the nudging frequency and X' is the difference to a reference field X_{ref} ($X' = X_{ref} - X$). The horizontal bar indicates a temporal filter that selects the low frequencies, so that gravity waves (considered high frequencies) are not damped by the nudging. The temporal filter is calculated by:

$$\frac{\partial \bar{X}'}{\partial t} = \lambda^{LF} \left(X_{ref} - X - \bar{X}' \right) \tag{5}$$

with the following numeric scheme:

$$\bar{X}'(t + \Delta t) = \left(1 - \Delta t \lambda^{LF}\right) \bar{X}'(t) + \Delta t \lambda^{LF} \left(X_{ref}(t) - X(t) \right) \tag{6}$$

whose filtering properties are detailed in Grebenkov and Serror (2014). Note that the possibility of oscillations during the transient solution produced by the coupling of Eq. 4 and Eq. 5 is eliminated by the following condition on λ^R:

$$\lambda^R = 0 \qquad if X' \bar{X}' < 0 \tag{7}$$

Otherwise, the value for λ^{relax}, λ^R and λ^{LF} are constant parameters and can be found in the Table S1.

References

Arakawa, A., & Lamb, V. R. (1981). A potential enstrophy and energy conserving scheme for the shallow water equations. *Monthly Weather Review*, *109*(1), 18–36.

Costa, A., Doglioli, A. M., Marsaleix, P., & Petrenko, A. A. (2017). Comparison of in situ microstructure measurements to different turbulence closure schemes in a 3-d numerical ocean circulation model. *Ocean Modelling*, *120*, 1–17.

Damien, P., Bosse, A., Testor, P., Marsaleix, P., & Estournel, C. (2017). Modeling postconvective submesoscale coherent vortices in the northwestern m editerranean s ea. *Journal of Geophysical Research: Oceans*, *122*(12), 9937–9961.

Estournel, C., Marsaleix, P., & Ulses, C. (2021). A new assessment of the circulation of atlantic and intermediate waters in the eastern mediterranean. *Progress in Oceanography*, *198*, 102673.

Grebenkov, D. S., & Serror, J. (2014). Following a trend with an exponential moving average: Analytical results for a gaussian model. *Physica A: Statistical Mechanics and its Applications*, *394*, 288–303.

Griffies, S. M., & Hallberg, R. W. (2000). Biharmonic friction with a smagorinsky-like viscosity for use in large-scale eddy-permitting ocean models. *Monthly Weather Review*, *128*(8), 2935–2946.

Jackett, D. R., McDougall, T. J., Feistel, R., Wright, D. G., & Griffies, S. M. (2006). Algorithms for density, potential temperature, conservative temperature, and the freezing temperature of seawater. *Journal of Atmospheric and Oceanic Technology*, *23*(12), 1709–1728.

Kundu, P., Cohen, M. I., & Hu, H. H. (2004). *Fluid mechanics*. Amsterdam: Elsevier

Academic Press.

Leonard, B. P. (1979). A stable and accurate convective modelling procedure based on quadratic upstream interpolation. *Computer methods in applied mechanics and engineering*, *19*(1), 59–98.

Lyard, F. H., Allain, D. J., Cancet, M., Carrre, L., & Picot, N. (2021). Fes2014 global ocean tides atlas: design and performances. *Ocean Science Discussions*, *2021*, 140. Retrieved from `https://os.copernicus.org/preprints/os-2020-96/` doi: 10 .5194/os-2020-96

Marsaleix, P., Auclair, F., & Estournel, C. (2006). Considerations on open boundary conditions for regional and coastal ocean models. *Journal of Atmospheric and Oceanic Technology*, *23*(11), 1604–1613.

Marsaleix, P., Auclair, F., & Estournel, C. (2009). Low-order pressure gradient schemes in sigma coordinate models: The seamount test revisited. *Ocean Modelling*, *30*(2-3), 169–177.

Marsaleix, P., Auclair, F., Floor, J. W., Herrmann, M. J., Estournel, C., Pairaud, I., & Ulses, C. (2008). Energy conservation issues in sigma-coordinate free-surface ocean models. *Ocean Modelling*, *20*(1), 61–89.

Marsaleix, P., Michaud, H., & Estournel, C. (2019). 3d phase-resolved wave modelling with a non-hydrostatic ocean circulation model. *Ocean Modelling*, *136*, 28–50.

Pairaud, I. L., Auclair, F., Marsaleix, P., Lyard, F., & Pichon, A. (2010). Dynamics of the semi-diurnal and quarter-diurnal internal tides in the bay of biscay. part 2: Baroclinic tides. *Continental Shelf Research*, *30*(3-4), 253–269.

Pairaud, I. L., Lyard, F., Auclair, F., Letellier, T., & Marsaleix, P. (2008). Dynamics

of the semi-diurnal and quarter-diurnal internal tides in the bay of biscay. part 1: Barotropic tides. *Continental Shelf Research*, *28*(10-11), 1294–1315.

Siddorn, J., & Furner, R. (2013). An analytical stretching function that combines the best attributes of geopotential and terrain-following vertical coordinates. *Ocean Modelling*, *66*, 1–13.

Toublanc, F., Ayoub, N., Lyard, F., Marsaleix, P., & Allain, D. (2018). Tidal downscaling from the open ocean to the coast: a new approach applied to the bay of biscay. *Ocean Modelling*, *124*, 16–32.

Zaron, E. D. (2019). Baroclinic tidal sea level from exact-repeat mission altimetry. *Journal of Physical Oceanography*, *49*(1), 193-210. Retrieved from `https://doi.org/10.1175/JPO-D-18-0127.1` doi: 10.1175/JPO-D-18-0127.1

Zunino, P., Lherminier, P., Mercier, H., Daniault, N., García-Ibáñez, M. I., & Pérez, F. F. (2017). The GEOVIDE cruise in may–june 2014 reveals an intense meridional overturning circulation over a cold and fresh subpolar north atlantic. *Biogeosciences*, *14*(23), 5323–5342. doi: 10.5194/bg-14-5323-2017

Notes

1. available at `https://sites.google.com/view/symphonieoceanmodel/home`

Table S1. Numerical and physical constants used in SYMPHONIE. As the spatial resolution is the same for longitude and latitude, only one of them is described.

Name	Symbol	Value
Internal time step	Δt	90 s
External time step	Δt_{ext}	1.25 s
Mean spatial step	$\bar{\Delta x}$	900 m
Minimum spatial step	Δx_{min}	800 m
Maximum spatial step	Δx_{max}	1000 m
Number of layers	nz	60
Size of the sponge layer	D_{sponge}	70 grid nodes
Boundary nudging frequency for velocity	λ^{relax}	0.1 days
Nudging frequency for T,S	λ^{R}	2 days
Low frequency for nudging	λ^{LF}	10 days
Bottom roughness	z_0^b	1×10^{-3} m
Minimum friction coefficient	$C_{D\,min}$	2.5×10^{-3}

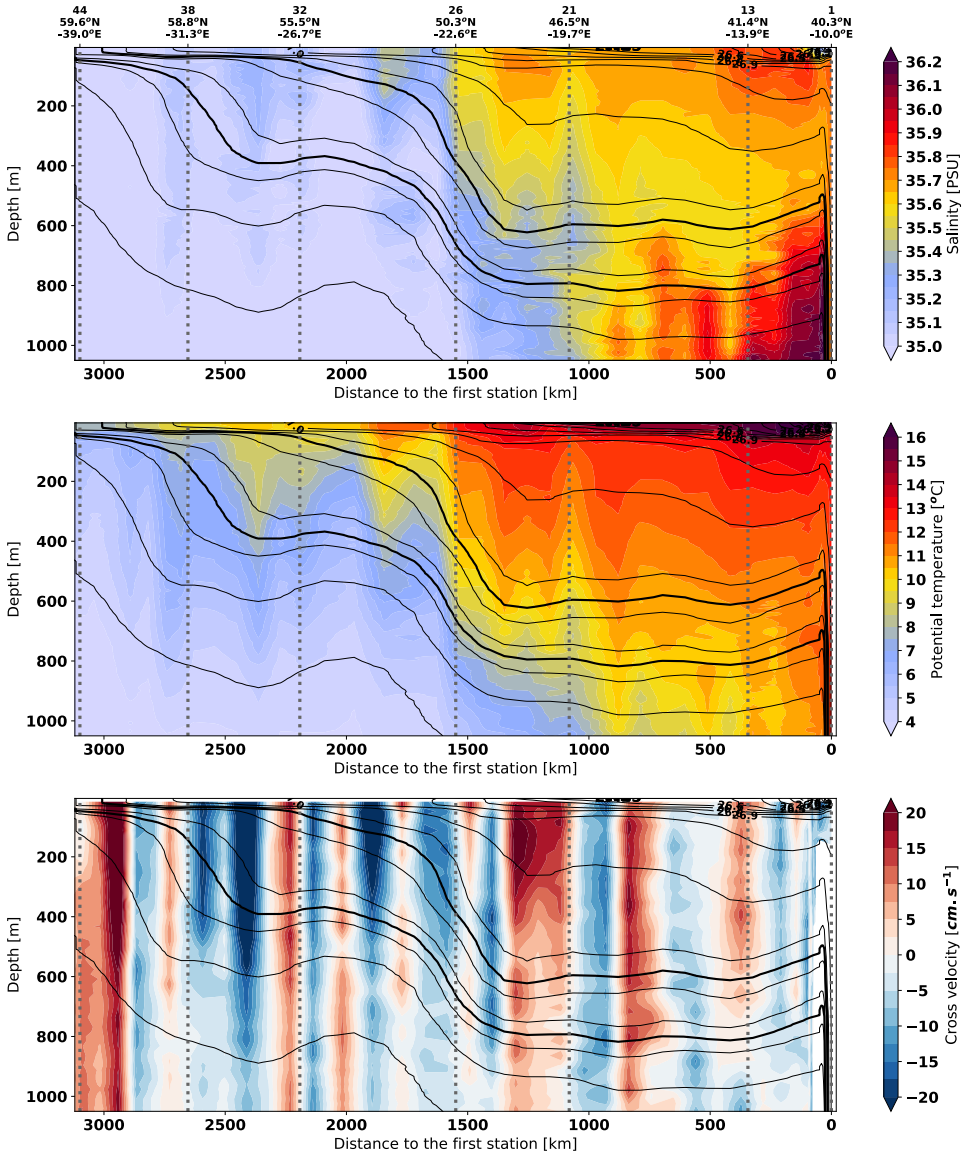

Figure S1. GEOVIDE measurements of (upper panel) the salinity, (central panel) the potential temperature and (lower panel) the velocity across the section from LADCP. The black lines represent the isopycnals of potential density anomaly. Each station where particles were sampled are represented by the dotted gray lines (station number and localization on top). Data from Zunino et al. (2017).

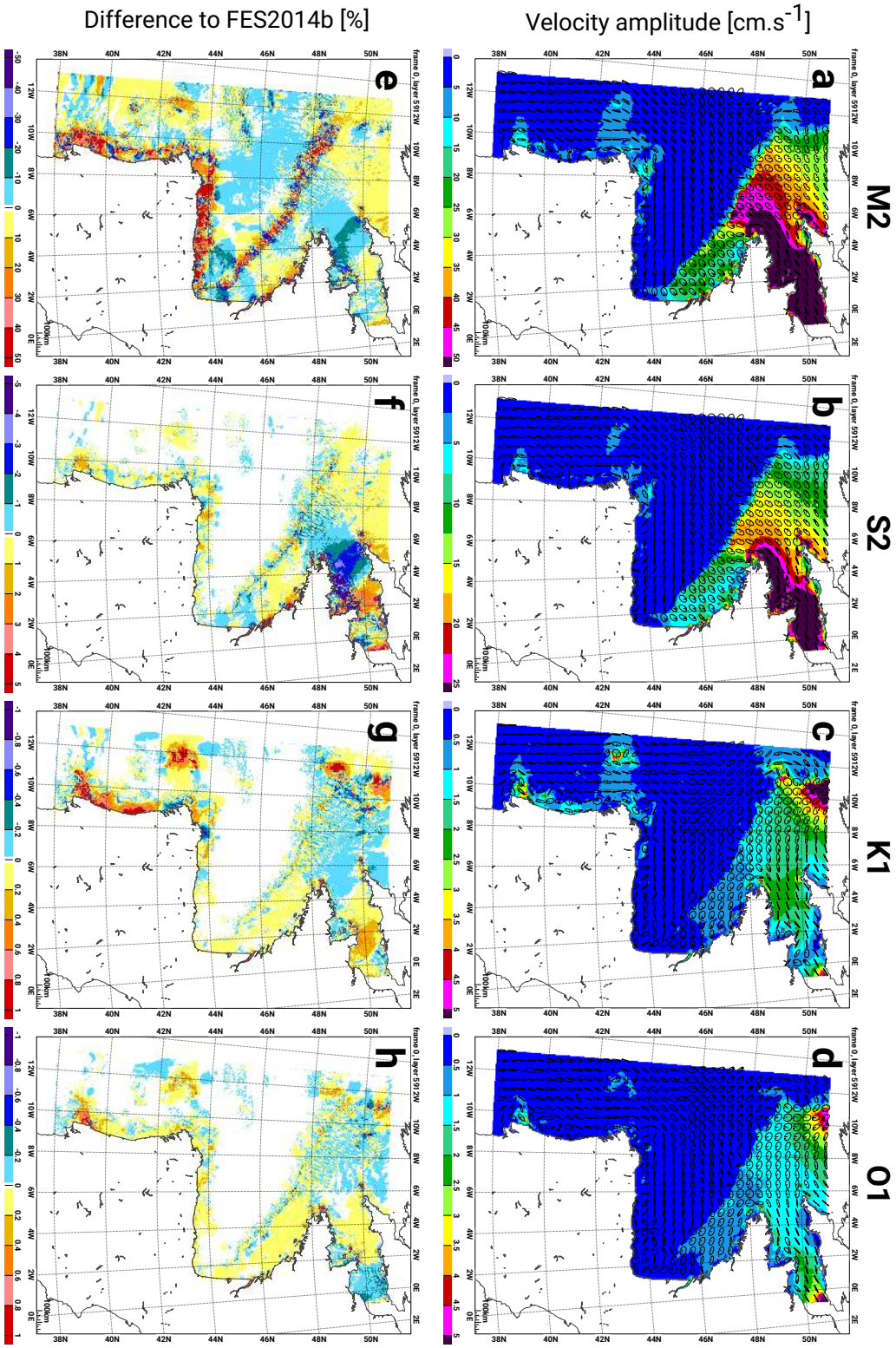

Figure S2. (a-e) Barotropic velocity amplitude for the simulated tidal harmonics and (f-j) the difference to FES2014b atlas (Lyard et al., 2021).

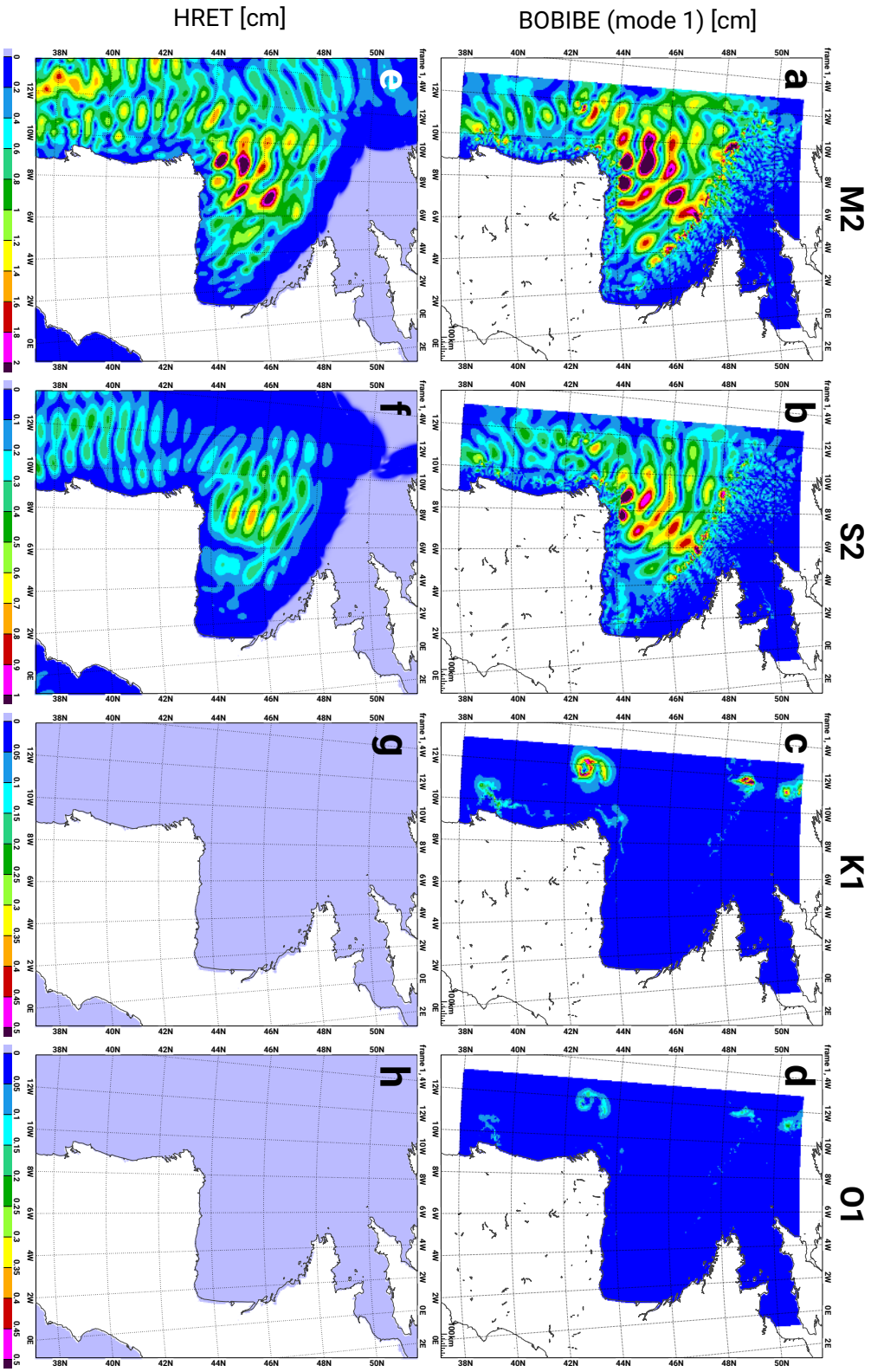

Figure S3. (a-d) Internal tide surface elevation amplitude for M2, S2, K1, O1 simulated tidal harmonics and (e-h) the corresponding value from HRET empirical IT atlas (Zaron, 2019).

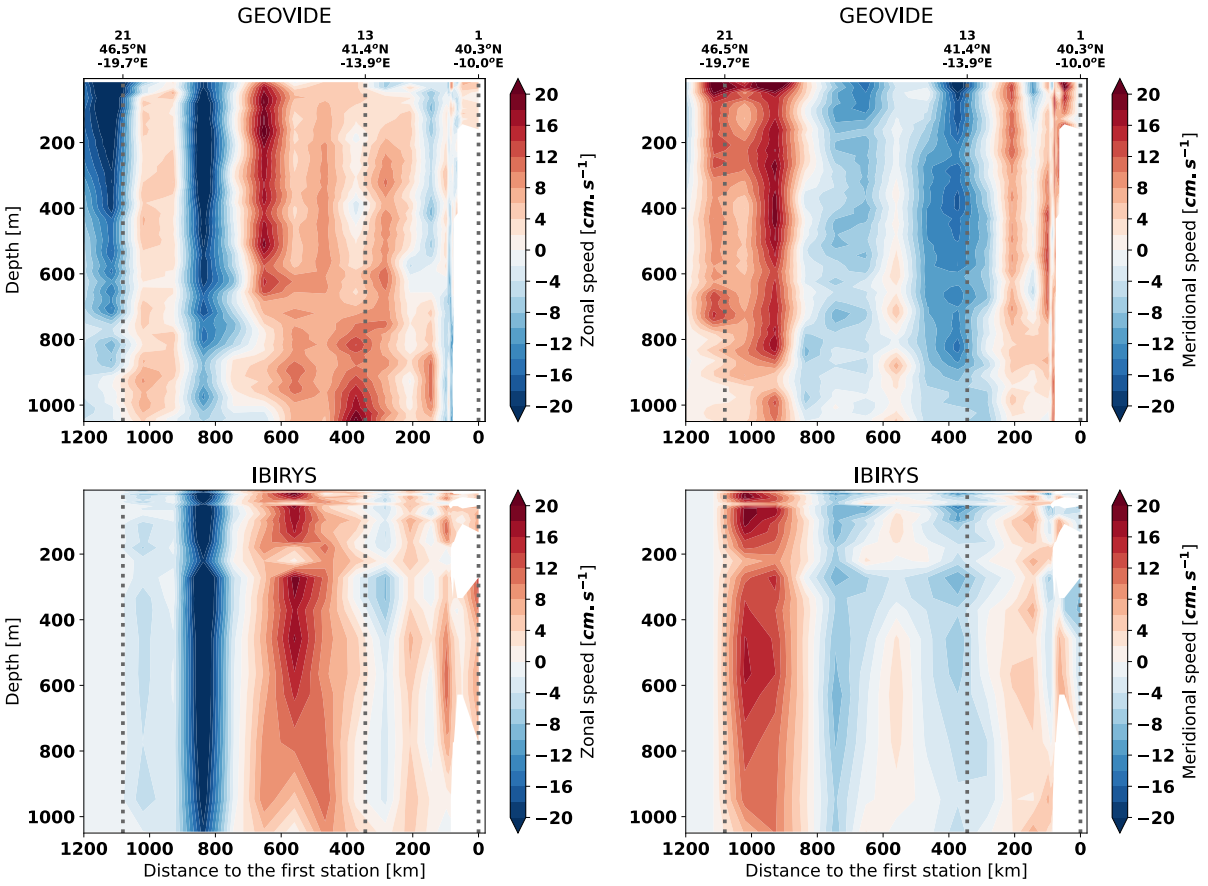

Figure S4. Vertical structure of the currents in the daily mean of IBIRYS12 reanalysis and GEOVIDE measurements. The values of IBIRYS12 are co-located (time and space) with the stations of the GEOVIDE cruise. GEOVIDE measurements from Zunino et al. (2017).

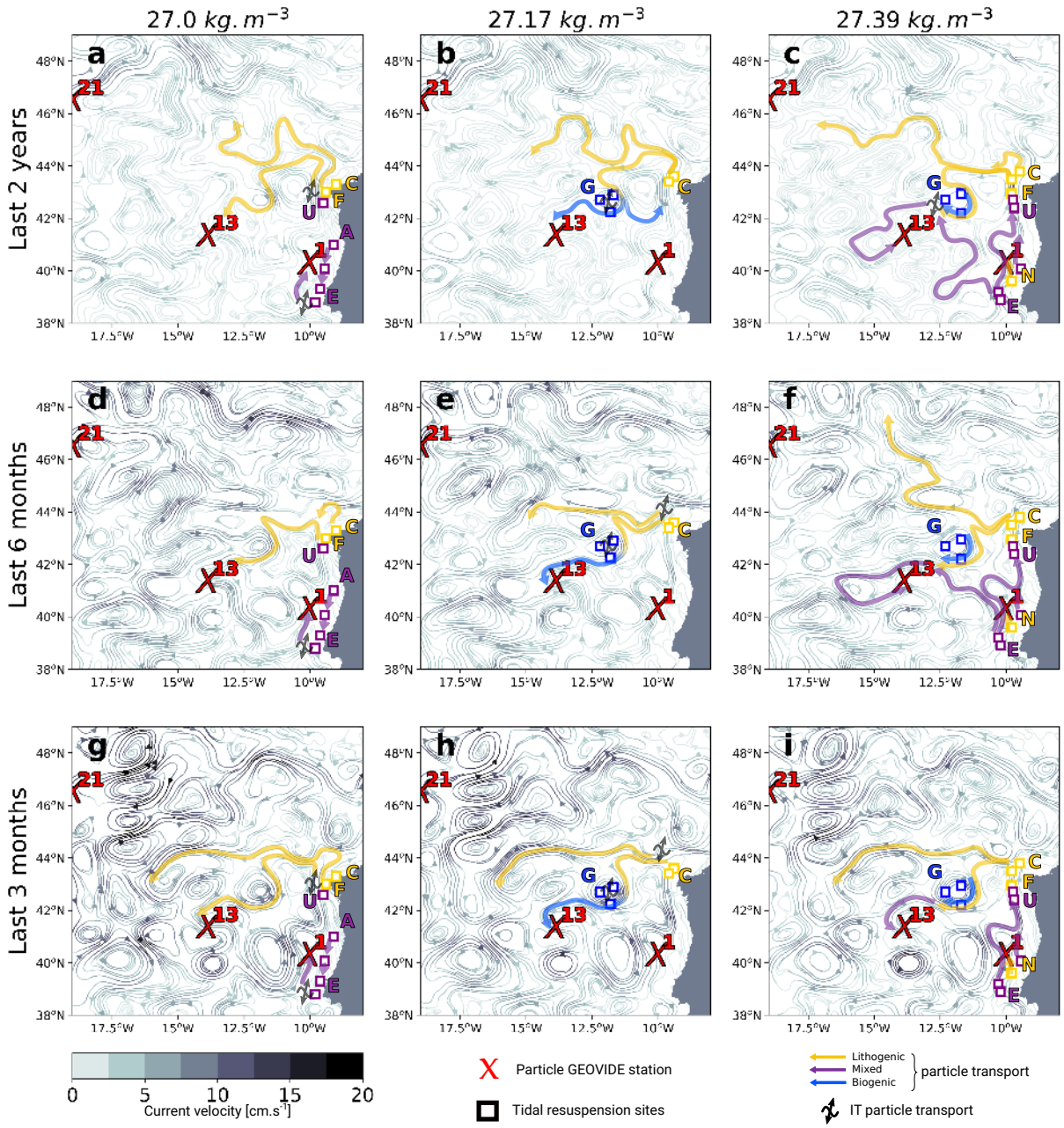

Figure S5. Streamline based on the mean velocity (top) 2 years, (center) 6 months and (bottom) 3 months before June 2014 at (left) 180 m, (middle) 500 m and 800 m. The red crosses show the GEOVIDE particle measurement stations. The squares show the location of tidal resuspension sites. The arrows describe the potential pathways of the particles from the tidal resuspension sites to the GEOVIDE stations. The colors define the nature of the particles transported: yellow for lithogenic, blue for biogenic and purple for both mixed.